IUTAM Symposium on Unsteady Separated Flows and their Control, June 18-22, 2007, Corfu, Greece

SIMULATION AND MODELLING OF A LAMINAR SEPARATION BUBBLE ON AIRFOILS

F. RICHEZ*, I. MARY, V. GLEIZE AND C. BASDEVANT
ONERA, Computational Fluid Dynamics and Aeroacoustics Department,
BP 72 - 29, avenue de la Division Leclec - 92322 Chatillon, France
* Francois.Richez@onera.fr

Introduction

Thanks to the Reynolds Averaged Navier-Stokes (RANS) approach, the calculation of flows around a whole aircraft is nowadays possible. However many studies seem to prove this approach is not mature for the prediction of complex flow phenomena. For example, numerical simulations of the flow around an airfoil at static and dynamic stall is still a very challenging task for CFD application. The phenomenon is caracterised by a massive flow separation on the suction side of the profile, which leads to a sudden drop of lift and an increase of the drag coefficient. The account of this phenomemon is important for the design of many industrial domains, such as helicopter rotor blades (retreating blade) or jet engines (rotating stall). Hence, because of manufacturing interest, the unsteady RANS (URANS) equation simulation has been widely used to compute dynamic stall flow. Unfortunately, the results are far from being totally reliable for predicting the dynamic stall behavior of airfoils and have a large computational cost. In this context, some researchers have chosen to start from scratch by considering static stall. They have proved that the solution is very sensitive to the grid resolution and to the turbulence model [1]. Even, when in the more simple case of static stall, the RANS equation simulation does not predict correctly the stall occurrence. Indeed, the flow over an airfoil near maximum lift combines different complex mechanisms which are still challenging the RANS methods. For thin airfoil profiles, the transition of the boundary layer usually happens close to the leading edge by a Laminar Separation Bubble (LSB). Next, the turbulent boundary layer remains attached on the middle area of the airfoil profile before separating near the trailing edge. Thereby, the massive flow separation of stall may result from the increase of the turbulent separation area or the breakdown of the LSB. In all cases, the effect of the LSB on the turbulent separation is strong, and its impact in the stall phenomenon is not negligible. This may be one of the reasons why the RANS approach, which is not able to accurately simulate transition, fails to predict stall occurrence. Last years, some studies have proved the Large Eddy Simulation (LES) provides an effective tool for tackling transitional and separated flow [2] [3]. Hence, we decided to achieve a LES of the flow around an airfoil near stall, with high resolution in the LSB. In this way, a numerical data base of the transitional flow could complete the experimental data, and be helpful for the improvement of the turbulence models. The numerical transitional flow is presented and analysed in the first part. In the second part, we study the ability of the RANS approach using a bubble transition criteria to simulate the flow in the LSB. Especially, the integral parameters and the Reynolds stresses are compared to the LES results.

1. LES of a LSB transition process at the leading edge of an airfoil

1.1. FLOW PARAMETERS AND NUMERICAL METHOD

Numerical method

The compressible Navier-Stokes equations are solved in a multibloc structured solver based on a finite volume method. Overlapping RANS and LES domains are used (see Figure 1). In the

RANS domain, the Spalart-Allmaras model is used in order to take into account the pressure side turbulent boundary layer. In the LES domain, the selective mixed scale model is used to represent the subgrid scale terms [4]. At each time step, the values of the conservative variables in the RANS domain of the overlapping zone are computed by averaging the LES variables in the cell volume of the RANS domain. Moreover these conservative variables are used to transport the turbulent viscosity of the Spalart-Allmaras model. The information transfer between the RANS domain and the LES one requires boundary conditions obtained using ghost cells and enrichment procedure [5].

The viscous fluxes are discretized by a second-order accurate centered scheme. For the Euler

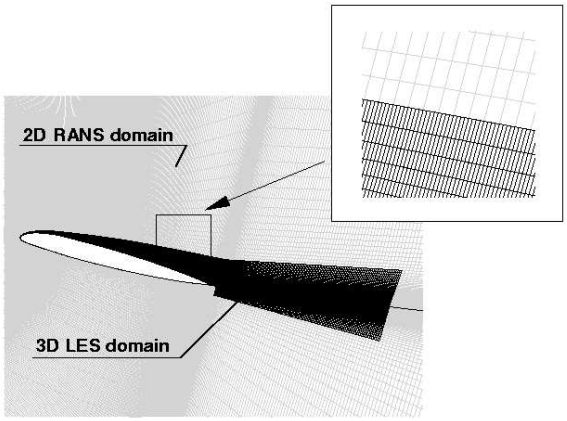

Figure 1. LES mesh.

fluxes discretization, a hybrid centered/upwind version of the AUSM+(P) scheme, whose dissipation is proportional to the local fluid velocity, is employed [6]. To improve the efficiency, an implicit time integration is employed to deal with the very small grid size encountered near the wall. Then a second order accurate three-level backward differentiation formula is used to approximate the temporal derivate. An approximate Newton method is used to solve the non-linear problem. At each iteration of the inner process, the resolution of the linear system relies on the Lower-Upper Symmetric Gauss-Seidel (LU-SGS) implicit method. These numerical methods have been developed at the ONERA in the FLU3M code and validated for several applied computations [6] [3].

Flow and computation parameters

The 2D helicopter fan blade OA209 profile has been retained for this study. The Reynolds number, based on the chord and the freestream velocity, is 1.8 million and the freestream Mach number is equal to 0.16. The angle of attack is 15 degrees which is, according to experimental studies achieved by the ONERA [7], just prior the stall occurrence.

The LES domain is located in the whole suction side of the boundary layer and in a region of one chord length in the wake zone (see Figure 1). Compared to the RANS domain, the LES grid is much refined in the streamwise direction and keeps the same resolution in the wall normal direction. In order to reduce the computational cost, the LES domain is decomposed into several sub-domains, which differ by their spanwise extent and spanwise resolution. The spanwise extent has been chosen in order to be greater than the boundary layer thickness along the profile [5]. At the interface between these domains, the shorter domain in the spanwise direction imposes the flow periodicity, since its information is duplicated in the ghostcells of the larger domain.

The mesh resolution usually required by LES for turbulent wall bounded flow is reached everywhere. The grid satisfies all along the suction side of the boundary layer the following conditions expressed in wall unit for, respectively, the streamwise, wall normal and spanwise directions: $\Delta x+ \leq 50$, $\Delta y+ \leq 2$ and $\Delta z+ \leq 15$.

However, simulate a transition process requires much more grid point density than simulate a turbulent flow. Hence, a particular attention has been given to the resolution in the transitional flow region, specially at the reattachment point of the LSB, which is the most difficult region of the flow to resolve. Only a few simulations of LSB with good resolution can be found in the literature. Alam & Sandham [8] have presented DNS of a LSB on a flat surface due to aspiration on the opposite boundary, while Yang & Voke [2] have carried out a LES of a LSB induced by a change of surface curvature. In table 1 we compare the mesh size in terms of wall units with these simulations. The grid spacings are evaluated at the skin friction peak, where the flow is more accuracy-demanding. The resolution is comparable to the DNS of Alam & Sandham in the streamwise direction, while it is slightly worse in the spanwise and wall-normal directions. Another check of resolution is the computation of the averaged subgrid eddy viscosity. It has been found that it is about 0.7 times the molecular viscosity at the reattachment point. This proves that the subgrid eddy viscosity has a small impact on the flow structures in this computation region. Hence, we can suppose that the resolution in the transitional flow region is not far away of what would be recognized as DNS.

The timestep is $3.10^{-5}c/U_0$, where c is the chord of the airfoil profile and U_0 the freestream

Case	Δx^+	Δy^+	Δz^+
Alam & Sandham	20.7	0.9	6.2
Yang & Voke	30.5	1	9
present LES	20	1.5	15

Table 1. Grid resolution at the skin friction peak compared with other simulations.

velocity. The code is parallelized using a domain decomposition technique based on the openMP directive. The computation has been running at 13 Gflops on four processors NEC SX5 during several thousand total CPU hours to ensure that the unsteady solution fluctuates around a steady averaged state. The statistical variables presented thereafter have been computed during the last five periods of the vortex shedding occuring at the trailing edge.

1.2. MAIN CHARACTERISTICS OF THE FLOW

Aerodynamics characteristics

Table 1 shows the lift and the drag coefficients calculated by the LES and compared to experimental data [7] and two fully turbulent (FT) RANS simulations using the Wilcox k-ω (k-ω) model [9] and the Menter Baseline (BSL) model [10]. The k-ω model is used with the Zheng modification [11] in order to alleviate the dependency of the model to the freestream ω value. These RANS simulations have been computed with the same RANS grid as shown on figure 1 (composed of 1259×101 grid points) and the same modified AUSM+(P) scheme has been employed. A grid convergence study has shown that the RANS solution is grid independent using this numerical method. One can see the RANS simulation using k-ω model gives almost the same lift value as the experiment, while the LES and the BSL slightly under-estimate its value. Futhermore, both RANS simulations provide a lower value of drag while the LES has the opposite effect. The temporal evolution of the LES lift and drag coefficients (not presented here) shows some oscillations, due to a vortex shedding at the trailing edge. The frequency of this phenomenon corresponds to a Strouhal number (based on the freestream velocity U_0 and the boundary layer thickness at the trailing edge δ_{te}) of $S_t = f \times \delta_{te}/U_0 \approx 0.2$ as expected. During the last periods of the vortex shedding, the lift seems to oscillate around a constant value, insuring the solution to be statistically converged.

Figure 2 shows the pressure distribution. One can see the LES provides a lower pressure plateau

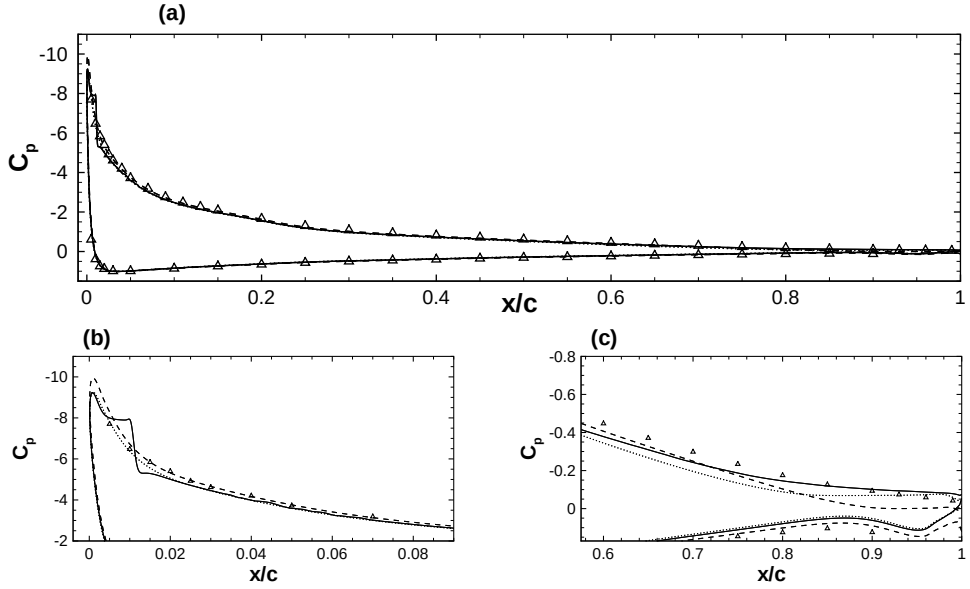

Figure 2. Pressure coefficient distribution on the whole airfoil surface (a), near the leading edge (b) and at the trailing edge (c). △, experiment; —, LES; - - -,k-ω FT; ·····, BSL FT.

	Experiment	LES	k-ω FT	BSL FT
Lift	1.416	1.366	1.415	1.377
Drag	0.029	0.039	0.023	0.024

Table 2. Experimental and numerical lift and drag coefficients.

value than the RANS k-ω simulation at the trailing edge. This is in good agreement with the experiment. The BSL model gives the more extended turbulent separated flow region. On the bulk airfoil profile, the pressure coefficient seems slightly over-estimated by the LES and the BSL, while, using k-ω model, the C_p curve matches well with the experimental measurements. However, the k-ω model over-estimates the velocity peak value at the leading edge, where both LES and BSL give a smaller peak value. At least, one can see that LES provides a flattened shape of the C_p distribution at the leading edge, which is characteristic of a LSB. No such shape is observed for the FT RANS simulations because the premature increase of the turbulent viscosity at the leading edge prevents the flow from separating. It might be disappointing to see the experimental C_p values do not show any evidence of a LSB. But it is well-known that the LSB extent is very sensitive to the freestream turbulence intensity and to the surface roughness [12]. It seems likely that the LSB size is reduced in the experiment because the external perturbations intensity is stronger, which moves upstream the transition process and the reattachment of the boundary layer.

Main characteristics of the LSB

As shown by the negative value of the mean skin friction (see Figure 3), the laminar boundary layer separates at $x = 0.3\%$ in the LES case. Several intantaneous skin friction plots have shown that the laminar separation point is fixed in time, while the flow is highly unsteady at the reattachment point. The averaged length L_b of the LSB is 1.3% of chord and $80 \times \delta_S^*$, where δ_S^* is the displacement thickness at the separation point. The transition of the boundary layer in the vicinity of the mean reattachment point is followed by a steep increase of the skin friction, which attains a higher value than for the fully turbulent flow case (represented in dashed line on Figure 3). Figures 4 shows the streamwise evolution of the integral momentum thickness θ/c in the transitional flow region. One can see that the momentum thickness is almost constant in the separated flow and

suddenly grows at the reattachement point, to reach a larger value than for the fully turbulent flow case. This emphasizes the large thicknening effect of the LSB on the turbulent boundary layer, which might make the turbulent separation at the trailing easier to arise.

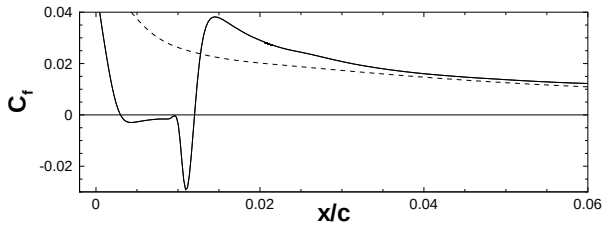

Figure 3. Skin friction coefficient in the transitional flow region. —, LES; - - -,k-ω FT.

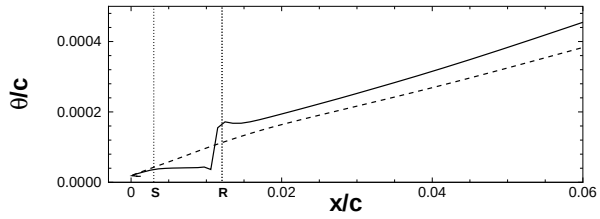

Figure 4. Momentum thickness θ/c in the transitional flow region. —, LES; - - -,k-ω FT.

1.3. Flow structures in the transitional et reattaching flow region

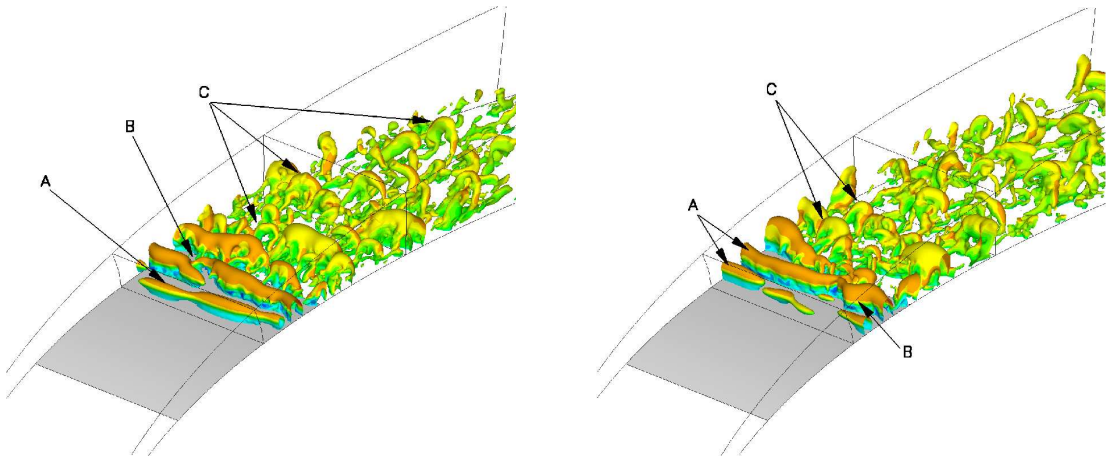

Figure 5. Isosurface of negative instantaneous pressure fluctuations p' colored by the streamwise velocity. The two plots have been taken at two different times. Grey region represents the mean extent of the LSB.

Instability mechanism

Figure 5 shows isosurfaces of negative instantaneous pressure fluctuations colored by the streamwise velocity. One can see that 2D structures (labelled A), characterized by a particular wave number, appear in the second half of the LSB. It seems that these vortices result from an inviscid instability of the shear layer. Indeed, the mean velocity profile in the LSB has an inflection point, which is a sufficient condition for an inviscid instability. No perturbations have been introduced into the laminar flow in order to trigger the transition. But the inflectional flow is most likely unstable enough, to quickly amplify the small disturbances coming from the numerical truncation

errors. In order to check this assumption, the present simulated results are compared with linear instability theory [13].
The Fourier transforms of the streamwise velocity signals at different locations along the bubble have been computed. The velocity spectra have shown that fluctuations, essentially composed of the frequency $f = 90000Hz$, appear in the LSB and quickly grow when convected along the bubble until non-linear effects lead to a large bandwidth spectrum.
Then, the incompressible stability features of several mean velocity profiles have been analysed, solving the Orr-Sommerfeld equation. These profiles have been taken where the perturbations amplitude was small enough in order to be considered as basic flow. Then, the spatial linear analysis reveals that the most unstable mode is characterized by the same frequency as found in the LES. Futhermore, increasing the value of the Reynolds number in the Orr-Sommerfeld equation leads to the same results, which indicates that this disturbance results from a 2D inviscid instability mechanism. Good agreement of the spatial growth rate of the unstable mode is also found between LES and linear theory, as shown on figure 6.

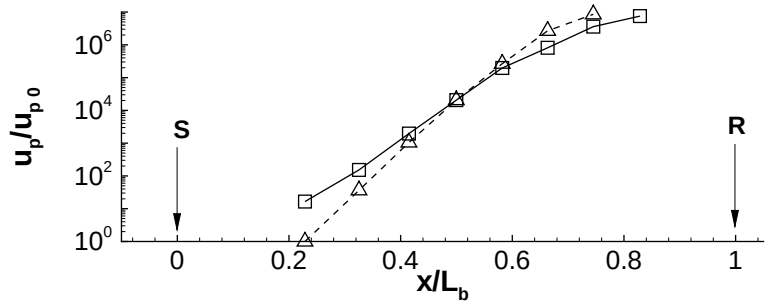

Figure 6. Spatial growth of the most unstable mode. □, LES; △, Linear instability analysis.

Breakdown to turbulence

As indicated by the changing slope of the curves, close to the reattachment point, on figure 6, the unstable mode amplitude saturates as the non-linear terms become significant. Figure 5 shows that three-dimensional structures rapidly appear from the reattachment point. The extremely suddenness of the breakdown to turbulence makes its mechanism difficult to analysed. However, the isosurfaces of negative instantaneous pressure fluctuations seem to show that the 2D vortices (A) become distorted in the spanwise direction as indicated by the label (B). This distortion process gives rise to hairpin vortices (C) near the mean reattachment point. These hairpin structures are still visible downstream. The spanwise extent of the emerging hairpin vortices at the reattachment point has the same order of magnitude of the spanwise distortion wave length. It is hence most likely that the distorted structures (B) change continuously into hairpin vortices, as the flow reattaches to the wall. Futhermore, as shown by Roshko (1981) and also observed by Yang & Voke [2], this spanwise wave length of 3D structures (B) seems to be roughly the same as the streamwise wave length of 2D mode vortices (A).

Relaxing boundary layer

The turbulent boundary layer at the reattachment point is different from an equilibrium turbulent boundary layer. Because the pressure gradient is still very strong at the reattachment point, typical turbulent boundary layer features are reached downstream a slow relation region. This non-equilibrium zone can be seen on figure 7. The red lines represent the low speed streaks in the sub-layer region ($y^+ = 10$). In a typical turbulent boundary layer, these streaks are long and

stretched in the streamwise direction. One can see that the streaks are short and irregular from the reattachment point up to some distance downstream ($x/c \approx 0.01 - 0.03$), and exhibit the turbulent characteristic pattern from $x/c \approx 0.04$.

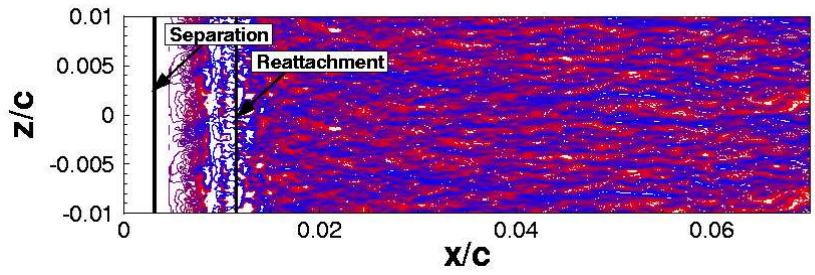

Figure 7. Contours of positive (blue) and negative (red) streamwise velocity fluctuations in the plane $y^+ = 10$. The domain is duplicated in the spanwise direction.

2. RANS modelling of the transition induced by a LSB

2.1. Description of the method

The ability of different turbulence models to handle the transitional flow in a LSB on airfoil are studied in this section. The k-ω model with and without SST correction [10] and the BSL model have been retained in this section to test the influence of a Bubble Transition Criteria (BTC) in RANS simulations. This criteria consists on computing the laminar part length l_{lam} of the LSB using a semiempirical method proposed by Roberts [12]:

$$\frac{l_{lam}}{\theta_S} = 25000 \frac{log[cotanh(0.1732 \times Tu)]}{Re_{\theta_S}}$$

where Tu is the freestream turbulence level expressed in percent ($Tu = 0.1\%$ is used), θ_S is the momentum thickness at the separation point and Re_{θ_S} is the Reynolds based on θ_S and the freestream velocity at the separation point.
To impose the flow laminar before this transition location, an intermittency function γ is used:

$$\gamma = \begin{cases} 0 & \text{in the laminar flow region,} \\ 1 & \text{in the turbulent flow region.} \end{cases}$$

This intermittency function is used to switch off both the turbulence viscosity and the production terms of the turbulence variables in the laminar flow region. The wall boundary value for ω is also set to zero in the laminar region. Otherwise, high values of ω would be convected into the shear layer of the LSB and prevent the high production of turbulence kinetic energy expected at the reattachement point. This would tragically delay the transition process and lead to a highly overestimated LSB length. Thanks to this correction of the wall boundary value, peaks of both the turbulence kinetic energy and the turbulence viscosity are observed at the computed transition point, and reattachment occurs close downstream.

2.2. Results and analysis

The modeled Reynolds stresses obtained in the LSB and downstream the reattachment point are compared to the simulated Reynolds stresses obtained from LES on Figure 8. One can see the

LES Reynolds stresses maximum is reached at the mean reattachment point and equal to $-0.10 \times \rho_0 U_0^2$. This value is different for each turbulence model. The mean difference is due to the SST correction, which limit the eddy viscosity peak value near the reattachment point. Without the SST limitor, both k-ω and BSL models predict about a LES Reynolds stresses peak value twice larger. As the SST correction acts as a limitation of the eddy viscosity, the modeled Reynolds stresses peak value, on figure 8(c) is half the LES value. These differing turbulence intensities in the transitional flow region lead to differing downstream turbulent boundary layer features. Figure 9 shows the streamwise evolution of the displacement and the momentum thickness. For all cases, the displacement thickness δ_1/c attains a maximum level in the LSB where the reverse flow intensity is maximum. Both k-ω and BSL models provide lower maximum values than the LES, while the k-ω SST peak value prediction is very close to the LES. Then, δ_1/c decreases as the flow is about to reattach. After the reattachment point, the displacement thickness grows in the turbulent flow region. At $x/c = 10\%$, the displacement thickness is smaller with the BTC case than with the FT case, using k-ω model. The same effect can be observed with the BSL model. It seems that the over-estimated eddy viscosity peak value at the transition point, leads to the refinement of the turbulent boundary layer thickness from the reattachment point, instead of its expected thickening. The effect is observed up to the trailing edge. Then, with both k-ω and BSL models cases, the lift coefficient is higher using the BTC than for the FT case (see table 3). However, with the SST correction, the BTC has a thicknening effect on the turbulent boundary layer downstream the reattachement point, which leads to a smaller lift coefficient compared to the FT case (see table 3). Futhermore, using k-ω SST model, the displacement thickness curve reaches the LES one from 10% of chord, although it predicts a higher value at the reattachment point. Looking at the right-hand side plots on figure 9, one can see the evolution of the momentum

	k-ω	k-ω SST	BSL
FT	1.416	1.416	1.38
BTC	1.44	1.37	1.416

Table 3. Lift coefficient for the FT and BTC cases using different turbulence models.

thickness in the transitional flow region. Every model provides the same momentum thickness in the LSB, which remains constant up to the reattachment point. This is consistant with the small streamwise variation of the edge boundary layer velocity and the low friction value in the LSB. At the reattachment point, both the skin friction and the pressure coefficient quickly increase, which leads to a steep drop of the momentum thickness. As already observed looking at the displacement thickness, both k-ω and BSL models predict a lower θ_{11}/c with the BTC case than with the FT case. Using the SST correction, the BTC leads to higher value of θ_{11}/c compared to the FT case, which is in better agreement with the LES results. Then, because of the thickener turbulent boundary layer, the lift is decreased compared to the FT case, and reaches 1.37 which is very close to the LES value (see table 2).

Conclusion

LES of the flow around an airfoil profile at high angle of attack has been achieved, with a very high resolution in the transitional flow region near the leading edge. We have observed, in this LES, that the transition occurs in a LSB. The transition mechanism that the flow undergoes in and downstream the LSB has been analysed. This LES predicts the growth of 2D inviscid unstable modes. Both frequency and spatial growth rate are in good agreement with linear instability analysis. The quick breakdown of these 2D structures occurs owing to a spanwise distortion, which gives rise to hairpin vortices in the emerging turbulent boundary layer. The visualizations of these different structures are in good agreement with other high-resolved simulations of LSB. The data base of the transitional flow near the LSB, provided by this LES, has been used for the improvement of the transition prediction using RANS turbulence models. A criteria based on the laminar extent

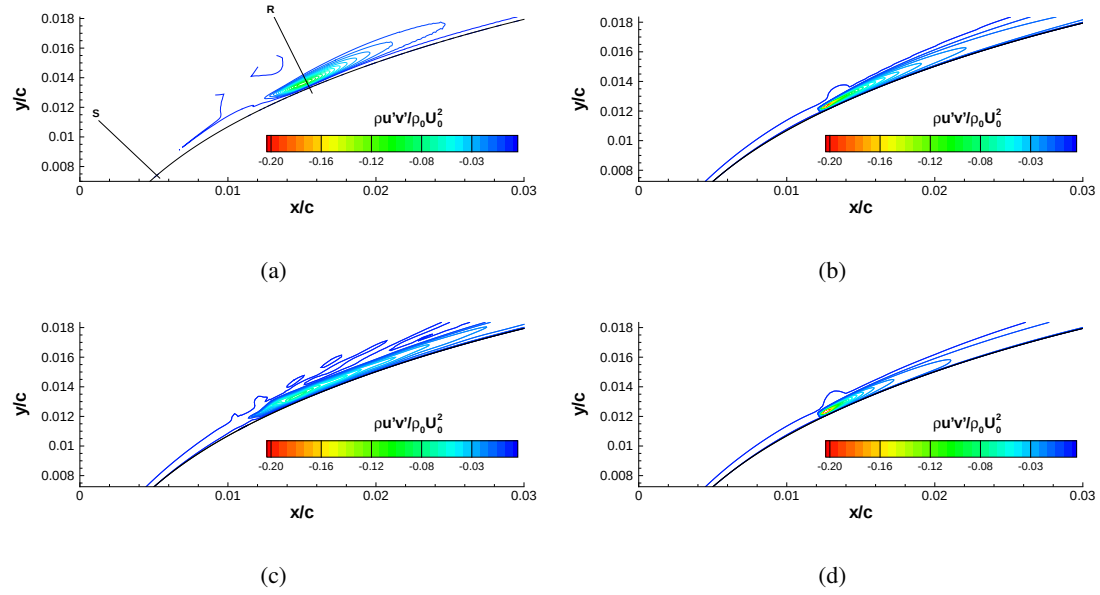

Figure 8. Reynolds stresses $\overline{\rho u' v'}/\rho_0 U_0^2$ contours in the transition flow region for: (a) LES, (b) k-ω, (c) k-ω SST, (d) BSL.

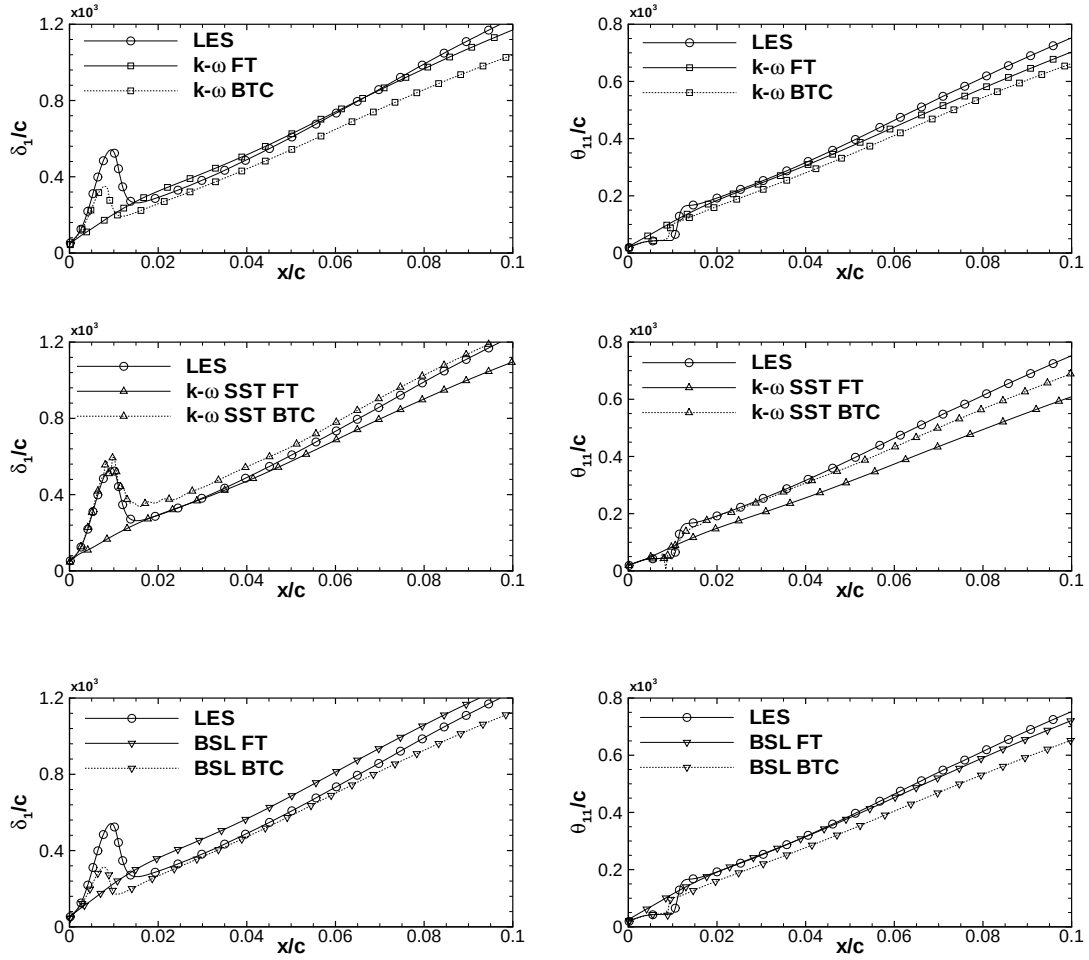

Figure 9. Integral displacement thickness δ_1/c and momentum thickness θ_{11}/c in the transitional flow region.

of the LSB is used to model the transition process. The ability of the k-ω and the BSL models to describe the transitional flow has been studied. The modeled Reynolds stresses peak value at the reattachment point is over-estimated in both cases, and the boundary layer downstream the LSB is refined instead of being thickened. Using the SST correction, the modeled Reynolds stresses peak value at the reattachment point is limited and we observe the expected thicknening of the boundary layer downstream the reattachment point.

References

[1] Gleize, V., Szydlowski, J., and Costes, M., "Numerical and physical analysis of turbulent viscous flow around a NACA0015 profile at stall," *European Congress on Computational Methods in Applied Sciences and Engineering*, Jyväskylä, Finland, 2004.

[2] Yang, Z. and Voke, P. R., "Large-eddy simulation of boundary-layer separation and transition at a change of surface curvature," *Journal of Fluid Mechanics*, Vol. 439, 2001, pp. 305–333.

[3] Raverdy, B., Mary, I., Sagaut, P., and Liamis, L., "High-resolution large-eddy simulation of the flow around a low pressure turbine blade," *AIAA Journal*, Vol. 41, No. 3, 2003, pp. 390 – 397.

[4] Lenormand, E., Sagaut, P., Ta Phuoc, L., and Comte, P., "Subgrid-scale models for large-eddy simulations of Compressible Wall Bounded Flows," *AIAA Journal*, Vol. 38, No. 8, August 2000, pp. 1340–1350.

[5] Mary, I. and Nolin, G., "Zonal grid refinement for large eddy simulation of turbulent boundary layers," *AIAA Paper 2004-0257*, Reno, US, 2004.

[6] Mary, I. and Sagaut, P., "LES of a flow around an airfoil near stall," *AIAA Journal*, Vol. 40, No. 6, 2002, pp. 1139 – 1145.

[7] Pailhas, G., Houdeville, R., Barricau, P., Le Pape, A., Faubert, A., Loiret, P., and David, F., "Experimental investigation of dynamic stall," *31th European Rotorcraft Forum*, September Florence, Italy, 2005.

[8] Alam, M. and Sandham, N. D., "Direct numerical simulation of 'short' laminar separation bubbles with turbulent reattachment," *Journal of Fluid Mechanics*, Vol. 410, 2000, pp. 1 – 28.

[9] Wilcox, D. C. and Rubesin, M. W., "Reassessment of the scale-determining equation for advanced turbulence models," *AIAA Journal*, Vol. 26, No. 11, November 1988, pp. 1299–1310.

[10] Menter, F. R., "Two-equation eddy-viscosity transport turbulence model for engineering applications," *AIAA Journal*, Vol. 32, No. 8, August 1994, pp. 1598–1605.

[11] Zheng, X., Liao, C., Liu, C., Sung, C. H., and Huang, T. T., "Multigrid computation of incompressible flows using two-equations turbulence models," *Journal of Fluids Engineering*, Vol. 119, December 1997, pp. 893–905.

[12] Roberts, W. B., "Calculation of laminar separation bubbles and their effect on airfoil performance." *AIAA Journal*, Vol. 18, No. 1, 1980, pp. 25 – 30.

[13] Schmid, P. J. and Henningson, D. S., *Stability and transition in shear flows*, Springer-Verlag, 2001.